

Multistrange Hyperon Production on Nuclear Targets

G.H. Arakelyan^{1†}, C. Merino², and Yu.M. Shabelski³

¹A.Alikhanyan National Scientific Laboratory (Yerevan Physics Institute)
Yerevan, 0036, Armenia
E-mail: argev@mail.yerphi.am

²Departamento de Física de Partículas, Facultade de Física
Instituto Galego de Física de Altas Enerxías (IGFAE)
Universidade de Santiago de Compostela, Galiza, Spain
E-mail: carlos.merino@usc.es

³Petersburg Nuclear Physics Institute
NCR Kurchatov Institute
Gatchina, St.Petersburg 188300 Russia
E-mail: shabelsk@thd.pnpi.spb.ru

Abstract

We consider the experimental data on yields of protons, strange Λ 's, and multistrange baryons (Ξ , Ω), and antibaryons production on nuclear targets, and the experimental ratios of multistrange to strange antibaryon production, at the energy region from SPS up to LHC, and compare them to the results of the Quark-Gluon String Model calculations. In the case of heavy nucleus collisions, the experimental dependence of the $\bar{\Xi}^+/\bar{\Lambda}$, and, in particular, of the $\bar{\Omega}^+/\bar{\Lambda}$ ratios, on the centrality of the collision, shows a manifest violation of quark combinatorial rules.

PACS. 25.75.Dw Particle and resonance production

† Deceased

1 Introduction

The Quark-Gluon String Model (QGSM) [1, 2, 3, 4] is based on the Dual Topological Unitarization (DTU), Regge phenomenology [5], and nonperturbative notions of QCD [6].

In QGSM, high energy interactions are considered as proceeding via the exchange of one or several Pomerons. The cut of at least some of those Pomerons determines the inelastic scattering amplitude of the particle production processes, that occur through the production and subsequent decay of the quark-gluon strings resulting from the cut of the Pomerons.

In the case of interaction with a nuclear target, the Multiple Scattering Theory (Gribov-Glauber Theory) [7] is used. For nucleus-nucleus collisions, the Multiple Scattering Theory allows to consider these interactions as the superposition of independent nucleon-nucleon interactions.

At very high energies, the contribution of enhanced Reggeon diagrams (percolation effects) becomes important, leading to a new effect, the suppression of the inclusive density of secondaries [8] into the central (midrapidity) region. This effect corresponds to a significant fusion of the primarily produced quark-gluon strings.

The QGSM provides a successful thorough description of multiparticle production processes in hadron-hadron [9, 10, 11, 12, 13], hadron-nucleus [14, 15, 16], and nucleus-nucleus [17, 18, 19, 20] collisions, for a wide energy region. In particular, the inclusive spectra of charged pions, kaons, nucleons, and Λ hyperons, were correctly described in the cited papers.

The production of multistrange hyperons, Ξ^- (dss), and Ω^- (sss), has special interest in high energy particle and nuclear physics. Since the initial-state colliding projectiles contain no strange valence quarks, all particles in the final state with non-zero strangeness quantum number should have been created in the process of the collision. This makes multistrange baryons a valuable probe in understanding the particle production mechanisms in high energy collisions. A remarkable feature of strangeness production is that the production of each additional strange quark featuring in the secondary baryons, i.e., the production rate of secondary $B(qqs)$ over secondary $B(qqq)$, then of $B(qss)$ over $B(qqs)$, and, finally, of $B(sss)$ over $B(qss)$, is affected by one universal strangeness suppression factor, λ_s :

$$\lambda_s = \frac{B(qqs)}{B(qqq)} = \frac{B(qss)}{B(qqs)} = \frac{B(sss)}{B(qss)}, \quad (1)$$

together with some simple quark combinatorics [21, 22, 23].

In the present paper, we compare the results of the standard QGSM calculations, with the experimental data on yields of p , Λ , Ξ , and Ω baryons, and the corresponding antibaryons, in nucleus-nucleus collisions, for a wide energy region, going from SPS up to LHC ranges.

We also consider the ratios of multistrange to strange antihyperon production in nucleus-nucleus collisions with different centralities, at CERN-SPS and RHIC energies.

In the standard formulation of QGSM, it is assumed that each secondary particle is produced by the independent fragmentation of one single quark-gluon string.

Let us define:

$$R(\bar{\Xi}^+/\bar{\Lambda}) = \frac{dn}{dy}(A + B \rightarrow \bar{\Xi}^+ + X) / \frac{dn}{dy}(A + B \rightarrow \bar{\Lambda} + X), \quad (2)$$

$$R(\bar{\Omega}^+/\bar{\Lambda}) = \frac{dn}{dy}(A + B \rightarrow \bar{\Omega}^+ + X) / \frac{dn}{dy}(A + B \rightarrow \bar{\Lambda} + X). \quad (3)$$

The produced antihyperons, $\bar{\Xi}^+$ and $\bar{\Omega}^+$, contain valence antiquarks newly produced during the collision. The ratios in eqs. (2) and (3) are reasonably described by QGSM when a relatively small number of incident nucleons participate in the collision (nucleon-nucleus collisions, or peripheral nucleus-nucleus collisions).

The number of quark-gluon strings (cut pomerons) in nucleus-nucleus collisions increases with the centrality of the collision, but if the secondaries are independently produced in a single quark-gluon string, the ratio of yields of different particles should not depend on the centrality.

However, in this paper we show that in central nucleus-nucleus collisions already at 158 GeV/c per nucleon, the experimental yield of multistrange hyperons is significantly larger than in peripheral collisions, indicating that the ratios in eqs. (2) and (3) strongly depend on the centrality of the collision. This effect decreases with the growth of the initial energy.

2 Other Models

Already in ref. [24], the UA1 Collaboration found, by measuring the strangeness yields in $p\bar{p}$ collisions at $\sqrt{s}=630$ GeV, that the strangeness suppression factor seemed to show a tendency to increase slowly with \sqrt{s} , effect that it was conjectured it could be due to the increase in the radiation of gluons which fragment into $s\bar{s}$ pairs.

On the other hand, by using the event generator LUCIAE to analyse the data by the NA35 Collaboration on the \bar{p} and $\bar{\Lambda}$ yields, in pp and central sulphur-nucleus collisions at 200A GeV, Sa and Tai indicated [25] that those data might imply the reduction of strangeness suppression in ultrarelativistic nucleus-nucleus collisions comparing to the nucleon-nucleon case at the same energy. Since the hadronic rescattering forcefully plays a role in the deficit of strangeness suppression, the authors then claimed the necessity of going further in the study of the reduction of strangeness suppression, before using it as a signal of quark-gluon plasma (QGP).

The NeXus approach is used in ref. [26] to analyse strangeness production in pp collisions at SPS and RHIC energies, to find that strangeness production is suppressed in proton-proton collisions at SPS energy, as compared to e^+e^- annihilation, while strangeness production in high energy pp and e^+e^- collisions agree quantitatively. The authors claim that the strangeness suppression in pp collisions at SPS is a consequence of

the limited-space available in string fragmentation at these energies. Thus, if the hadron mass is small as compared to the typical string energy, the hadron multiplicity ratios (e.g. strange to not-strange), reach asymptotic values, and a further increase of the string energy leads only to an overall increase of the produced hadron multiplicity, leaving their relative ratio unchanged. If, on the contrary, the string mass becomes comparable to the hadron masses (when the energy of the collision is smaller), the production of the heavy hadrons is suppressed due to the very limited phase space available.

In [27], Tounsi and Redlich [27] claimed that the pattern of enhancement of strange and multistrange baryons observed by the WA97 Collaboration could be understood on the basis of the significant role of canonical suppression in strangeness enhancement. By presenting quantitative predictions for the relative enhancement of Λ , Ξ , and Ω yields in the energy range from $\sqrt{s}=8.7$ GeV to $\sqrt{s}=130$ GeV, they showed that in the canonical approach strangeness enhancement is a decreasing function of collision energy, where the enhancement of Ω , Ξ , and λ would be of the order 100, 20, and 3, respectively. Strangeness enhancement is already seen at low energies, and found to be a decreasing function of collision energy in a set of data on the K^+/π^+ ratio, in AA relative to pp collisions. Such a behavior with the energy of the collision could also be expected for multistrange baryons, and, in fact, a statistical model implementing canonical strangeness conservation explains [28] the WA97 pattern and predicts that the enhancement is a decreasing function of collision energy. As an example, Tounsi and Redlich predict that at RHIC enhancement of Ω is smaller than at SPS, in contrast with the predictions by the UrQMD model of an enhancement at RHIC larger by a factor of four than at SPS [29]. It was also stressed the fact that the NA57 Collaboration data [30] which measure the yield per participant in Pb+Pb collisions relative to p+Pb and p+Be collisions show a saturation of the strangeness enhancement for a number of participant nucleons $N_{part} > 100$, while results of the NA57 Collaboration [31] indicated an abrupt change of Ξ^+ enhancement for lower values of N_{part} . Similar behavior had been previously seen on the K^+ yield measured by the NA22 Collaboration in Pb+Pb collisions [32].

In ref. [33], where it is pointed out that the correlation between strangeness enhancement and the J/Ψ anomalous suppression patterns observed in heavy ion collisions at top SPS energy $\sqrt{s}=17.2$ GeV, if studied as a function of the transverse size of the interaction region, makes considerably stronger the case for SPS being right at the onset of QGP formation, it is also found that the strangeness suppression factor varies considerably between the most central and the most peripheral bin in Pb+Pb collisions, being significantly smaller in central C+C and Si+Si than in Pb+Pb collisions, confirming the results of a previous analysis in ref. [34]. Thus, the strangeness suppression factor is larger in central light-ion collisions than in the most peripheral heavy-ion collisions, where it approaches the value found in pp collisions. These analyses raised the question on whether a regular behavior exists as a function of the system size in the strangeness production pattern in heavy ion collisions, either by taking λ_s as a function of the fraction of struck participants in the Glauber Model [34], either by looking for an underlying physical

mechanism implying the undersaturation of the strange phase space, with λ_s becoming an effective parametrization of a more complicated physical picture (i.e. see [35]).

In ref. [36], two different types of transport models, the microscopic transport model UrQMD, and a stochastic transport model provided by an elaborated transport cascade, were used to show that both dynamically account for the suppression in the yields of rare strange particles in $\pi\pi$ collisions, provided in the canonical formulation of the Boltzmann equation, and associated with the exact conservation of an U(1)-charge. The reason is that any kaon in the system requires the existence of a corresponding anti-kaon due to strangeness conservation, thus the probability of finding a particle anti-particle pair turns into a highly correlated conditional probability, the enhanced annihilation probability then leading to the canonical suppression in the kaon yields, behavior automatically included in the considered transport models.

As a matter of fact, and as noticed in [37], the value of strangeness suppression factor λ_s is measured and calculated by different methods. Thus, it has been considered as constant in energy range by Malhotra and Orava [38], while there are other analyses which accept the decrease of strangeness suppression with the increase of the collision energy [24, 39], and new Monte-Carlo event generators have been developed where λ_s is energy dependent [40].

The PYTHIA 6.4 predictions for strange particle spectra were calculated by Lobanov and collaborators [37] with new ATLAS tunes, to show that the analysis of particle yields in pp collisions at the LHC energies demonstrates the smaller strangeness suppression comparing with experiments at lower energies. Thus, the experimental data by the ALICE [41], CMS [42], and ATLAS [43] collaborations show a large increase in the measured production cross section of strange particles as \sqrt{s} increases from 0.9 to 7 TeV.

The UA1 Collaboration found a value of $\lambda_s=0.29$ from their measurements on the ratio K/π at energy $\sqrt{s}=630$ GeV, in agreement with previous measurements [38], and with UA5 and CDF experiments. Then they made energy dependence fitting for λ_s , and found a value $\lambda_s=0.31$ at the LHC energy of 14 TeV. From LHC data [41, 42, 43], in the range $\sqrt{s}=0.9$ to 7 TeV, in the central rapidity region, Lobanov and collaborators obtain an estimation of $\lambda_s=0.39$. They conclude that LHC data show an increase of strangeness production (or smaller strangeness suppression), with respect to previous experimental data in lower energy ranges.

Finally, H. Satz signaled [44] that in a hydrodynamical scenario the (universal) strangeness suppression factor for hadroproduction in high energy pp , pA , and AA collisions increases from 0.5 to 1.0 in a narrow temperature range around the quark-hadron transition temperature, and strangeness suppression disappears with the onset of color deconfinement, and with the onset of the full equilibrium resonance gas behavior.

3 Production of Secondaries in the QGSM

The QGSM [2, 9] provides quantitative predictions of different features of multiparticle production, in particular, of the inclusive densities of different secondaries, both in the

central, and in the beam fragmentation regions. In QGSM, high energy hadron-nucleon collisions are implemented through the exchange of one or several Pomerons, all elastic and inelastic processes resulting from cutting between (elastic) or through (inelastic) Pomerons [45].

Each Pomeron corresponds to a cylindrical diagram, and thus, when cutting one Pomeron, two showers of secondaries are produced (see figs. 1a and 1b).

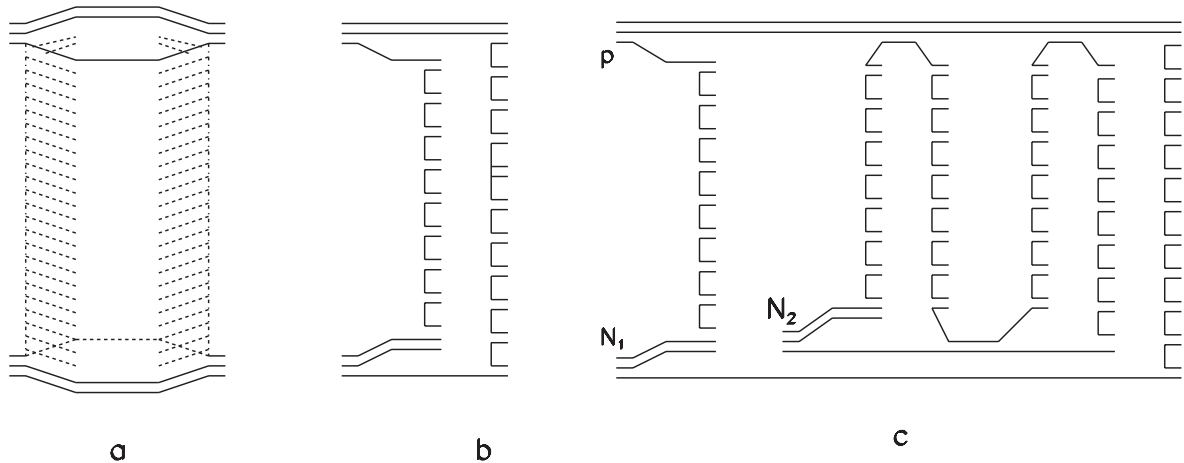


Figure 1: (a) Cylindrical diagram representing the Pomeron exchange within the DTU classification. Quarks are shown by solid lines; (b) Cut of the cylindrical diagram corresponding to the single-Pomeron exchange contribution in inelastic pp scattering; (c) Diagram corresponding to the inelastic interaction of an incident proton with two target nucleons, N_1 and N_2 , in a pA collision.

The inclusive spectrum of a secondary hadron h is then determined by the convolution of the diquark, valence quark, and sea quark distribution functions, $u(x, n)$ (every one normalized to unity), in the incident particles, with the fragmentation functions $G^h(z)$ for quarks and diquarks to contribute to the production of the secondary hadron h . Both the distribution functions and the fragmentation functions are constructed by using the well established Reggeon counting rules [46].

In particular, when $n > 1$, i.e. in the case of multipomeron exchange, the distributions of valence quarks and diquarks are softened due to the appearance of a new contribution from sea quark-antiquark pairs.

The details of the model are presented in [2, 9, 10, 11]. The average number of exchanged Pomerons slowly increases with the energy of the collision. The values of the Pomeron parameters used in the calculations presented in this paper have been taken from [10].

For a nucleon target, the inclusive rapidity, y , or Feynman- x , x_F , spectrum of a secondary hadron h has the form [2]:

$$\frac{dn}{dy} = \frac{x_F}{\sigma_{inel}} \cdot \frac{d\sigma}{dx_F} = \sum_{n=1}^{\infty} w_n \cdot \phi_n^h(x) + w_D \cdot \phi_D^h(x) , \quad (4)$$

where the functions $\phi_n^h(x)$ determine the contribution of diagrams with n cut Pomerons,

w_n is the relative weight of this diagrams, and the term $w_D \cdot \phi_D^h(x)$ accounts for the contribution of diffraction dissociation processes.

For pp collisions:

$$\phi_n^h(x) = f_{qq}^h(x_+, n) \cdot f_q^h(x_-, n) + f_q^h(x_+, n) \cdot f_{qq}^h(x_-, n) + 2(n-1)f_s^h(x_+, n) \cdot f_s^h(x_-, n) , \quad (5)$$

$$x_{\pm} = \frac{1}{2}[\sqrt{4m_T^2/s + x^2} \pm x] , \quad (6)$$

where $m_T = \sqrt{m^2 + p_T^2}$ is the transverse mass of the produced hadrons, and f_{qq} , f_q , and f_s , correspond to the contributions of diquarks, valence, and sea quarks (antiquarks), respectively, The contributions of the incident particle and the target proton depend on the variables x_+ and x_- , respectively [2, 1, 4, 46].

The first two terms in Eq. (5) correspond to chains with valence quarks (diquarks) at the ends, while the last term is connected to chains stretched between sea quark-antiquark. The expression of the functions f in Eq. (5) is determined by the convolution of the diquark and quark distribution functions, with the fragmentation functions, e.g.,

$$f_i^h(x_{\pm}, k) = \int_{x_{\pm}}^1 u_i(x_1, k) G_i^h(x_{\pm}/x_1) dx_1 , \quad (7)$$

where $i = qq$ diquarks, q valence quarks, and \bar{q} valence antiquarks, and q_s sea quarks (\bar{q}_s sea antiquarks), respectively.

In the calculation of the inclusive spectra of secondaries produced in pA collisions, we should consider the possibility of one or several Pomeron cuts in each of the ν blobs of the proton-nucleon inelastic interactions (see Fig. 1c).

It is also essential to take into account all diagrams with every possible Pomeron configuration, and its corresponding permutations [2, 3, 18]. The diquark and quark distribution functions and the fragmentation functions are the same as in the case of a proton-nucleon, pN , interaction.

The process shown in Fig. 1c satisfies [47, 48, 49, 50] the condition that the absorptive parts of the hadron-nucleus amplitude are determined by the combination of the absorptive parts of the hadron-nucleon amplitudes.

For nucleus-nucleus collisions, in the fragmentation region of the projectile we use the approach presented in refs. [17, 18, 19], where the beam of independent nucleons of the projectile interacts with the target nucleus, what corresponds to the rigid target approximation [51] of the Glauber Theory. Correspondingly, in the target fragmentation region the beam of independent target nucleons interacts with the projectile nucleus. The results obtained in this approach for the two fragmentation regions coincide in the central region. When the initial energy is not very high, the corrections due to the implementation of energy conservation play here a very important role. This approach was used in [19] to obtain a successful description of the yields of π^{\pm} , K^{\pm} , p , and \bar{p} , in Pb+Pb collisions at 158 GeV per nucleon.

The superposition picture of QGSM gives a reasonable description [13, 14, 19] of the inclusive spectra on nuclear targets at energies $\sqrt{s} = 14\text{--}30$ GeV. At RHIC energies the situation drastically changes: while the spectra of secondaries produced in pp collisions are described by QGSM rather well [13], the RHIC experimental data for $Au+Au$ collisions [52, 53] give clear evidence of suppression effects that reduce the midrapidity inclusive density by about a factor two, when compared to the predictions based on the superposition picture [18, 54, 55]. This reduction can be explained by the inelastic screening corrections connected to multipomeron interactions [8] (see Fig. 2). All these

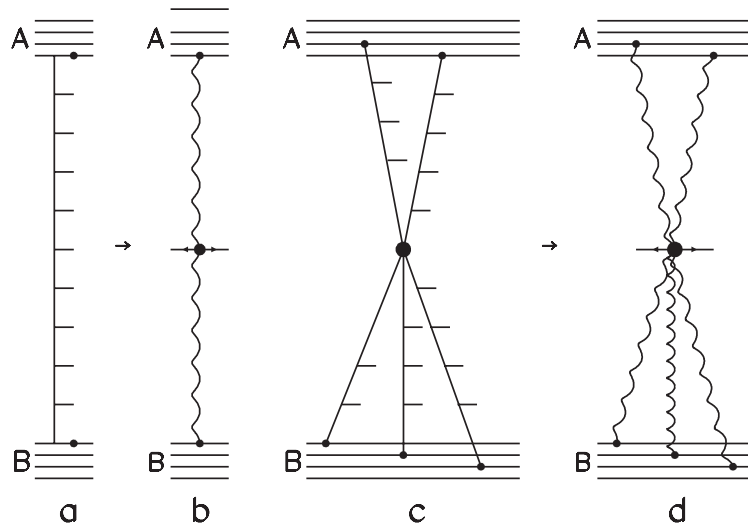


Figure 2: (a) Multiperipheral ladder diagram; (b) Inclusive cross section corresponding to diagram in (a); (c) Diagram with fusion of several ladders; (d) Inclusive cross section corresponding to diagram in (c).

diagrams are proportional to the squared longitudinal form factors of both colliding nuclei [8].

Though all numerical estimates are model dependent, since the numerical weight of the contribution of the multipomeron diagrams remains rather unclear due to the many unknown vertices in these diagrams, in some models the number of unknown parameters can be reduced. As an example of this, in reference [8] the Schwimmer model [56] was used to obtain consistent numerical predictions.

In order to account for the screening effects in the QGSM, it is technically more simple [13] to consider the maximal number of Pomerons, n_{max} , emitted by one nucleon in the central region. Then, after they are cut, these Pomerons lead to the different final states. Finally, the contributions of all diagrams with $n \leq n_{max}$ are accounted for, as at lower energies. The unitarity constraint also affects the emission of larger numbers of Pomerons, $n > n_{max}$, but due to fusion in the final state (at the quark-gluon string stage), the cut of $n > n_{max}$ Pomerons results in the same final state as the cut of n_{max} Pomerons.

By taking this approximation, all QGSM calculations become rather simple, straightforward, and very similar to those in the percolation approach [57, 58, 59]. .

4 Comparison of QGSM calculations with experimental data

4.1 Fixed Target Energy Data

The experimental data on proton and hyperon production were reasonably described in [16]. The data for p+Be and p+Pb collisions were also described in the same reference, but it appears that the value of the strange suppression parameter $\lambda_s=0.25$ would have to be slightly increased to get a better comparison with the experimental data. In the present paper we use the value $\lambda_s=0.32$, that provides good results for the description of the experimental data in references [60, 61]. The results of our calculation for p+Be and p+Pb collisions are presented in Table 1, where it is apparent the consistent agreement with the experimental data.

Process	$dn/dy, y \leq 0.5$ (Experimental Data)	dn/dy (QGSM)
$p + \text{Be} \rightarrow \Lambda$	$0.0334 \pm 0.0005 \pm 0.003$	0.0357
$p + \text{Be} \rightarrow \bar{\Lambda}$	$0.011 \pm 0.0002 \pm 0.001$	0.0128
$p + \text{Pb} \rightarrow \Lambda$	$0.060 \pm 0.002 \pm 0.006$	0.0678
$p + \text{Pb} \rightarrow \bar{\Lambda}$	$0.015 \pm 0.001 \pm 0.002$	0.0173
$p + \text{Be} \rightarrow \Xi^-$	$0.0015 \pm 0.0001 \pm 0.0002$	0.00261
$p + \text{Be} \rightarrow \bar{\Xi}^+$	$0.0007 \pm 0.0001 \pm 0.0002$	0.00113
$p + \text{Pb} \rightarrow \Xi^-$	$0.0030 \pm 0.0002 \pm 0.0003$	0.00336
$p + \text{Pb} \rightarrow \bar{\Xi}^+$	$0.0012 \pm 0.0001 \pm 0.0001$	0.00113
$p + \text{Be} \rightarrow \Omega^-$	$0.00012 \pm 0.00006 \pm 0.00002$	0.000143
$p + \text{Be} \rightarrow \bar{\Omega}^+$	$0.00004 \pm 0.00002 \pm 0.00001$	0.0000453
$p + \text{Pb} \rightarrow \Omega^-$	$0.00022 \pm 0.00008 \pm 0.00003$	0.000184
$p + \text{Pb} \rightarrow \bar{\Omega}^+$	$0.00005 \pm 0.00003 \pm 0.00002$	0.000058

Table 1: Experimental data by the NA57 Collaboration [69] on inclusive densities dn/dy of hyperon production in p+Be and p+Pb central $|y| \leq 0.5$ collisions at proton-nucleon 158 GeV/c, together with the results of the QGSM calculations ($\lambda_s = 0.32$).

In the case of Pb+Pb collisions at 158 GeV/c per nucleon, we compare the experimental data on dn/dy for central collisions ($|y| \leq 0.5$), measured by NA49 [62, 63, 64, 65, 66, 67], NA57 [68, 69], and WA97 [30] collaborations, with the corresponding QGSM predictions. The comparison for inclusive densities dn/dy of secondary proton and hyperons are shown in Table 2, where one can see that the experimental data obtained by each of the collaborations are, in general, compatible with those by the others.

The values in Table 2 state the reasonable description of the experimental data for secondary p , Λ , and $\bar{\Lambda}$, obtained in QGSM, by using the value $\lambda_s=0.32$, for the strangeness suppression factor, λ_s .

On the contrary, for the case of multistrange hyperon production of Ξ^- , $\bar{\Xi}^+$, Ω^- , and $\bar{\Omega}^+$, the values in Table 2 show that in the frame of the QGSM a correct description of the experimental data can only be obtained by using significant larger values of λ_s , i.e. by implementing a weaker suppression of strangeness production. This fact is a clear indication of a significant violation of the quark combinatorial rules [23, 22].

Process	Centrality	dn/dy, $ y \leq 0.4$ (Experimental Data)	dn/dy (QGSM)
Pb+Pb $\rightarrow p$	0–5%	29.6 ± 0.9 [62]	30.29
Pb+Pb $\rightarrow \Lambda$	0–10%	$9.5 \pm 0.1 \pm 1.0$ [65, 67]	6.64
Pb+Pb $\rightarrow \Lambda$	0–10%	$10.9 \pm 1.0 \pm 1.3$ [63, 67]	
Pb+Pb $\rightarrow \Lambda$	0–10%	13.7 ± 0.9 [67, 30]	
Pb+Pb $\rightarrow \bar{\Lambda}$	0–10%	$1.24 \pm 0.03 \pm 0.13$ [65, 67]	1.65
Pb+Pb $\rightarrow \bar{\Lambda}$	0–10%	$1.62 \pm 0.16 \pm 0.2$ [63, 67]	
Pb+Pb $\rightarrow \bar{\Lambda}$	0–10%	1.8 ± 0.2 [67, 30]	
Pb+Pb $\rightarrow \Xi^-$	0–5%	$2.08 \pm 0.09 \pm 0.21$ [67, 69]	1.458
Pb+Pb $\rightarrow \bar{\Xi}^+$	0–5%	$0.51 \pm 0.04 \pm 0.05$ [67, 69]	0.482
Pb+Pb $\rightarrow \Xi^-$	0–10%	1.5 ± 0.01 [67, 30]	1.34
Pb+Pb $\rightarrow \bar{\Xi}^+$	0–10%	0.37 ± 0.06 [67, 30]	0.443
Pb+Pb $\rightarrow \Xi^-$	0–10%	$1.43 \pm 0.33 \pm 0.16$ [66, 67]	1.34
Pb+Pb $\rightarrow \Xi^-$	0–10%	$1.44 \pm 0.10 \pm 0.15$ [65, 67]	1.34
Pb+Pb $\rightarrow \bar{\Xi}^+$	0–10%	$0.31 \pm 0.03 \pm 0.03$ [65, 67]	0.443
Pb+Pb $\rightarrow \Omega^-$	0–5%	$0.31 \pm 0.07 \pm 0.05$ [67, 69]	0.246
Pb+Pb $\rightarrow \bar{\Omega}^+$	0–5%	$0.16 \pm 0.04 \pm 0.02$ [67, 69]	0.111
Pb+Pb $\rightarrow \Omega^-$	0–10%	$0.14 \pm 0.03 \pm 0.01$ [64, 67]	0.197
Pb+Pb $\rightarrow \bar{\Omega}^+$	0–10%	$0.07 \pm 0.03 \pm 0.01$ [64, 67]	0.071
Pb+Pb $\rightarrow \Omega^-$	0–11%	$0.259 \pm 0.037 \pm 0.026$ [67, 68]	0.197
Pb+Pb $\rightarrow \bar{\Omega}^+$	0–11%	$0.129 \pm 0.0122 \pm 0.013$ [67, 68]	0.071

Table 2: The comparison of QGSM predictions with the experimental data on midrapidity yields of p , \bar{p} , strange Λ , $\bar{\Lambda}$, and multistrange Ξ^- , $\bar{\Xi}^+$, Ω^- , and $\bar{\Omega}^+$, produced at different centrality percentage in Pb+Pb collisions at energy 158 GeV/c per nucleon, measured by the NA49 [62, 63, 64, 65, 66, 67], NA57 [68, 69], and WA97 [30] collaborations. Experimental data presented in the review [67] are also considered. The values of the strangeness suppression factor, λ_s , used in the different QGSM calculations presented in this table, are the following: $\lambda_s=0.32$ (for p and Λ production), $\lambda_s=0.7$ (for Ξ production), and $\lambda_s=0.75$ (for Ω production).

Actually, the quark combinatorial rules assume that every strange quark can be picked up with the same probability, i.e. with the same value of λ_s , but comparison in Table 2 demonstrates the opposite picture: the value of the parameter λ_s for the cases of Ξ^- ,

Ξ^+ , Ω^- , and $\bar{\Omega}^+$ production appears to be more than 3 times larger than for the cases of Λ and $\bar{\Lambda}$ production.

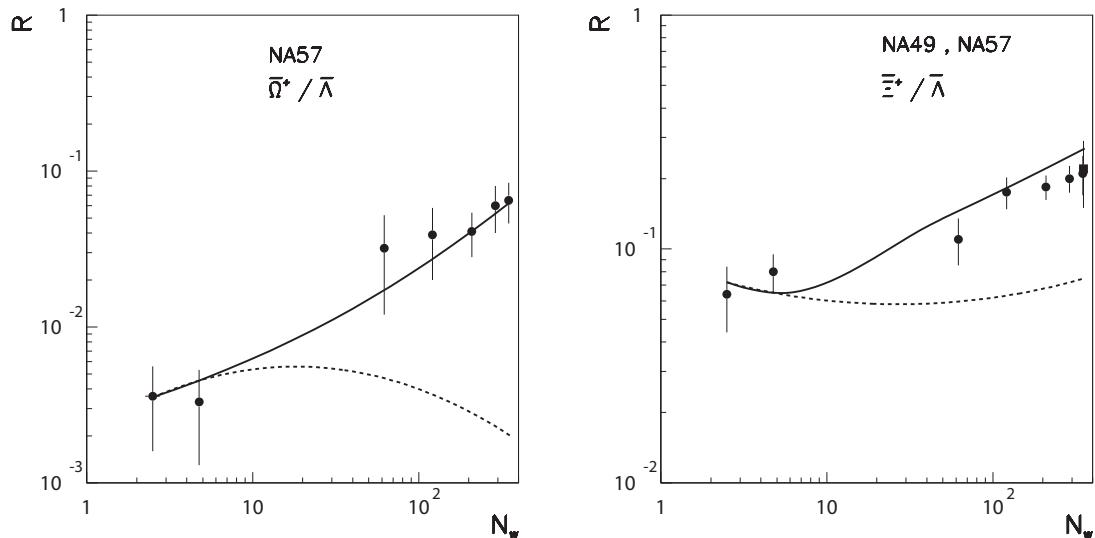


Figure 3: Ratios of $\bar{\Omega}^+ / \bar{\Lambda}$ (left panel), and of $\bar{\Xi}^+ / \bar{\Lambda}$ (right panel) as functions of the number of wounded nucleons, N_w . The experimental data of Pb+Pb collisions for different numbers of wounded nucleons, N_w (different centralities) measured by the NA57 Collaboration (points), and by the NA49 Collaboration (squares) are presented, and compared with the corresponding QGSM predictions.

In Fig. 3 we show the comparison of the QGSM prediction with the experimental data [69] on the dependence of the ratios $\bar{\Omega}^+ / \bar{\Lambda}$ (left panel) and $\bar{\Xi}^+ / \bar{\Lambda}$ (right panel), on the number of wounded nucleons, N_w , in Pb+Pb collisions at 158 GeV/c per nucleon. The number of wounded nucleons, N_w , is directly related to the centrality of collisions. Thus, small values of N_w correspond to peripheral collisions (large impact parameter), while large values of N_w corresponds to central collisions (small impact parameter).

At small values of N_w the ratio is practically equal to that in the cases of p+Be and p+Pb collisions, and all they can be correctly described by the QGSM by using a value of the strangeness suppression parameter, $\lambda_s=0.32$. Then, the experimental ratio increases rather fast with the increasing value of N_w , i.e. when we move from peripheral to central Pb+Pb collisions. This behavior is reasonably reproduced by the full line in Fig. 3, that it has been calculated with the value $\lambda_s=0.32$ at its left end, and with the values of λ_s shown in Table 2 at its right end.

The results of QGSM calculations with a constant value $\lambda_s=0.32$, disregarding of the value of the number of wounded nucleons (centrality), N_w , are shown in Fig 3 by dashed lines.

Obviously, for small values of N_w , both curves coincide, but when N_w increases the full line also increases in agreement with the data, while the dashed line is practically constant, with exception of small corrections mainly connected to energy conservation. This dashed line shows a very significant disagreement with the experimental data at large values of N_w .

The difference between the full and the dashed lines for the ratio $\bar{\Omega}^+/\bar{\Lambda}$ in a very central event is of about one order of magnitude. Such a large difference comes from the fact that the cross section for $\bar{\Omega}$ production is proportional to λ_s^3 .

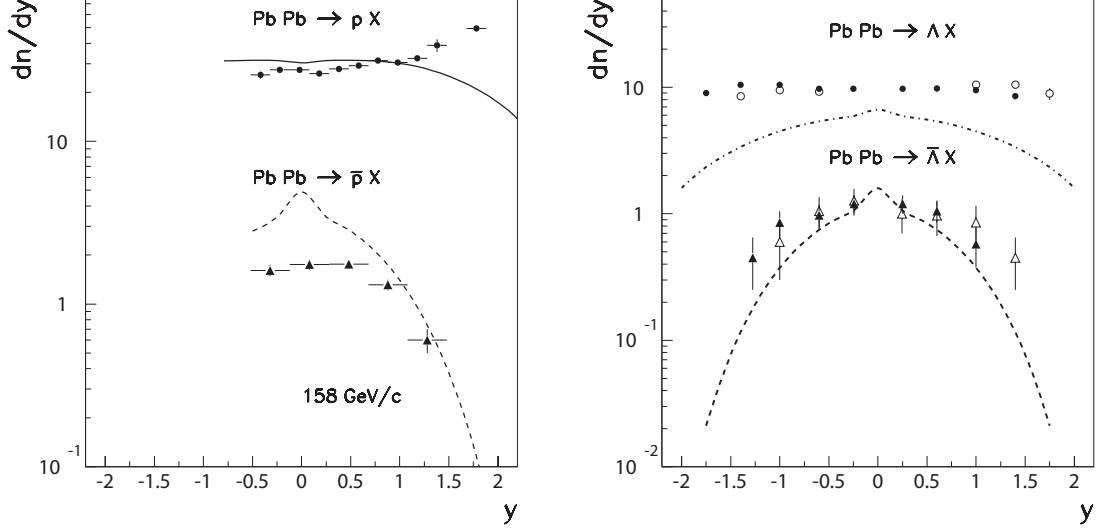


Figure 4: Rapidity dependence of dn/dy for p , \bar{p} (left panel), and for Λ , $\bar{\Lambda}$ (right panel) productions. The experimental data of Pb+Pb collisions measured by the NA49 Collaboration at 158 GeV/c per nucleon [65] are presented, and compared with the QGSM predictions (solid and dashed lines).

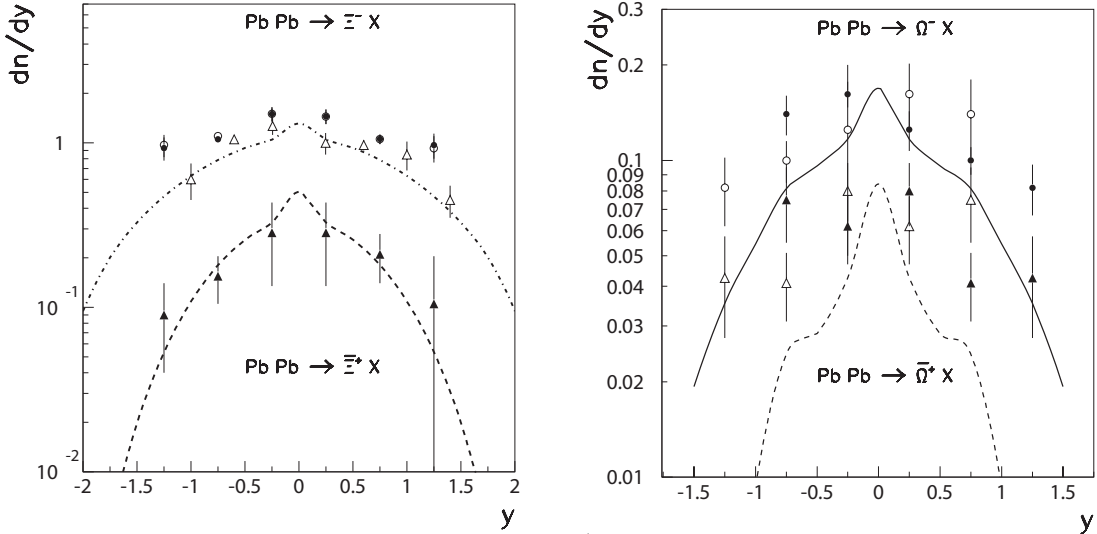


Figure 5: Rapidity dependence of dn/dy for Ξ^- , Ξ^+ (left panel), and Ω^- , Ω^+ (right panel) productions. The experimental data of Pb+Pb collisions measured by the NA49 Collaboration at 158 GeV/c per nucleon [64] are presented, and compared to the QGSM predictions (solid and dashed lines).

Meanwhile, since the cross section for Ξ^+ production is proportional to λ_s^2 , the difference between full and dashed curves for the ratio $\Xi^+/\bar{\Lambda}$ is not so large.

This behaviour in which the value of the strangeness suppression factor λ_s increases with the value of N_w (centrality), indicates that the simple quark combinatorial rules [23, 22] are not valid for central collisions of heavy nuclei.

In figs. 4 and 5, the rapidity dependence of p , \bar{p} , Λ , $\bar{\Lambda}$ (Fig. 4), and of Ξ^- , $\bar{\Xi}^+$, Ω^- , $\bar{\Omega}^+$ (Fig. 5) baryons production in central Pb+Pb collisions with initial momentum 158 GeV/c per nucleon, are shown, and compared with the QGSM predictions (full and dashed lines). The full and dashed lines have been calculated for baryon and antibaryon production by using the corresponding values of the strangeness suppression parameter, λ_s , given in Table 2.

Both in figs. 4 and 5, one can appreciate a reasonable agreement of the QGSM predictions with the experimental data for the production of all secondary baryons.

4.2 STAR Collaboration Data

Now we consider the experimental data on midrapidity densities of protons and hyperons in Au+Au and Cu+Cu collisions measured by the STAR [70, 71, 72, 73, 74] and PHENIX [75, 76] collaborations at RHIC energies, and we compare them with the results of the corresponding QGSM calculations. The comparison is presented in Table 3, where one can appreciate that, in general, the agreement of the QGSM predictions with the experimental data in this energy region is quite reasonable.

Again, we see here that the value of λ_s for multistrange hyperon production is larger than for the case of Λ and $\bar{\Lambda}$ production. Now this difference is not so large as it is for collisions at lower energies (see Table 2). Moreover, it seems that the difference in the value of the parameter λ_s decreases with the growing of the energy, meaning that the violation of the quark combinatorial rules becomes less important for high energy collisions.

In Fig. 6 we present the comparison of the QGSM predictions with experimental data on the N_w dependence of the ratios $\bar{\Omega}^+/\bar{\Lambda}$ (left panel), and $\bar{\Xi}^+/\bar{\Lambda}$ (right panel), measured by the STAR Collaboration in the midrapidity region, at $\sqrt{s} = 62.4$ GeV. Similarly as in Fig. 3, the left end of the full line here was calculated with a value $\lambda_s=0.32$, while for the right end the values of λ_s presented in Table 3 were used. The dashed line was calculated with a constant value of $\lambda_s=0.32$.

The same calculations for the ratio of $\bar{\Xi}^+/\bar{\Lambda}$ in Cu+Cu collisions at $\sqrt{s}=200$ GeV, are shown in Fig. 7. Here we see again that the violation of the quark combinatorial rules decreases with the growth of the energy of the collision, the difference between the full and dashed lines being of the order of the experimental error bars, at $\sqrt{s} = 200$ GeV.

Process	\sqrt{s} (GeV)	Centrality	dn/dy (Experimental Data)	dn/dy (QGSM)	λ_s
Au+Au $\rightarrow p$	62.4	0–5%	29.0 ± 3.8 [72]	22.826	0.32
Au+Au $\rightarrow \bar{p}$	62.4	0–5%	13.6 ± 1.7 [72]	15.115	
Au+Au $\rightarrow \Lambda$	62.4	0–5%	$15.7 \pm 0.3 \pm 2.3$ [73]	9.221	0.32
Au+Au $\rightarrow \bar{\Lambda}$	62.4	0–5%	$8.3 \pm 0.2 \pm 1.1$ [73]	6.258	
Au+Au $\rightarrow \Xi^-$	62.4	0–5%	$1.63 \pm 0.09 \pm 0.18$ [73]	1.406	0.4
Au+Au $\rightarrow \bar{\Xi}^+$	62.4	0–5%	$1.03 \pm 0.00 \pm 0.11$ [73]	0.996	
Au+Au $\rightarrow \Omega^-$	62.4	0–20%	$0, 212 \pm 0.028 \pm 0.018$ [73]	0.222	0.55
Au+Au $\rightarrow \bar{\Omega}^+$	62.4	0–20%	$0, 167 \pm 0.027 \pm 0.015$ [73]	0.154	
Au+Au $\rightarrow p$	130.	0–5%	28.2 ± 3.1 [72]	27.450	0.32
Au+Au $\rightarrow p$	130.	0–5%	28.7 ± 0.9 [76]	27.450	
Au+Au $\rightarrow \bar{p}$	130.	0–5%	20.0 ± 2.2 [72]	22.723	
Au+Au $\rightarrow \bar{p}$	130.	0–5%	20.1 ± 1.0 [76]	22.723	
Au+Au $\rightarrow \Lambda$	130.	MB	4.8 ± 0.3 [75]	3.379	0.32
Au+Au $\rightarrow \bar{\Lambda}$	130.	MB	4.3 ± 0.7 [75]	2.861	
Au+Au $\rightarrow \Lambda$	130.	0–5%	$17.3 \pm 1.8 \pm 2.8$ [75]	13.070	0.32
Au+Au $\rightarrow \Lambda$	130.	0–5%	$17.0 \pm 0.4 \pm 1.7$ [73]		
Au+Au $\rightarrow \bar{\Lambda}$	130.	0–5%	$12.7 \pm 1.82 \pm 2.0$ [75]	11.053	
Au+Au $\rightarrow \bar{\Lambda}$	130.	0–5%	$12.3 \pm 0.3 \pm 1.2S$ [73]		
Au+Au $\rightarrow \Xi^-$	130.	0–10%	$2.0 \pm 0.14 \pm 0.2$ [70]	1.976	0.39
Au+Au $\rightarrow \bar{\Xi}^+$	130.	0–10%	$1.70 \pm 0.12 \pm 0.17$ [70]	1.754	
Au+Au $\rightarrow \Omega^- + \bar{\Omega}^+$	130.	0–10%	$0.55 \pm 0.11 \pm 0.06$ [70]	0.544	0.48
Cu+Cu $\rightarrow \Lambda$	200	0–10%	4.68 ± 0.45 [74]	4.200	0.32
Cu+Cu $\rightarrow \bar{\Lambda}$	200	0–10%	3.79 ± 0.37 [74]	3.772	
Cu+Cu $\rightarrow \Xi^-$	200	0–10%	0.62 ± 0.08 [74]	0.559	0.33
Cu+Cu $\rightarrow \bar{\Xi}^+$	200	0–10%	0.52 ± 0.08 [74]	0.507	
Cu+Cu $\rightarrow \Omega^- + \bar{\Omega}^+$	200.	0–10%	0.141 ± 0.017 [74]	0.140	0.39
Au+Au $\rightarrow p$	200.	0–5%	34.7 ± 4.4 [72]	31.450	0.32
Au+Au $\rightarrow \bar{p}$	200.	0–5%	26.7 ± 3.4 [72]	27.765	
Au+Au $\rightarrow \Lambda$	200	0–5%	14.8 ± 1.5 [74]	15.762	0.32
Au+Au $\rightarrow \Lambda$	200	0–5%	$16.7 \pm 0.2 \pm 1.1$ [71]		
Au+Au $\rightarrow \bar{\Lambda}$	200	0–5%	11.7 ± 0.9 [74]	14.152	
Au+Au $\rightarrow \bar{\Lambda}$	200	0–5%	$12.7 \pm 0.2 \pm 0.9$ [71]		
Au+Au $\rightarrow \Xi^-$	200	0–5%	$2.17 \pm 0.06 \pm 0.19$ [71]	2.173	0.34
Au+Au $\rightarrow \bar{\Xi}^+$	200	0–5%	$1.83 \pm 0.05 \pm 0.20$ [71]	1.962	
Au+Au $\rightarrow \Omega^- + \bar{\Omega}^+$	200.	0–5%	$0.53 \pm 0.04 \pm 0.03$ [71]	0.525	0.4

Table 3: Experimental data on dn/dy by the STAR Collaboration [74] on p , \bar{p} , Λ , $\bar{\Lambda}$, Ξ^- , $\bar{\Xi}^+$ and Ω^- , $\bar{\Omega}^+$ production in central Cu+Cu and Au+Au collisions at RHIC energies, together with the corresponding QGSM results.

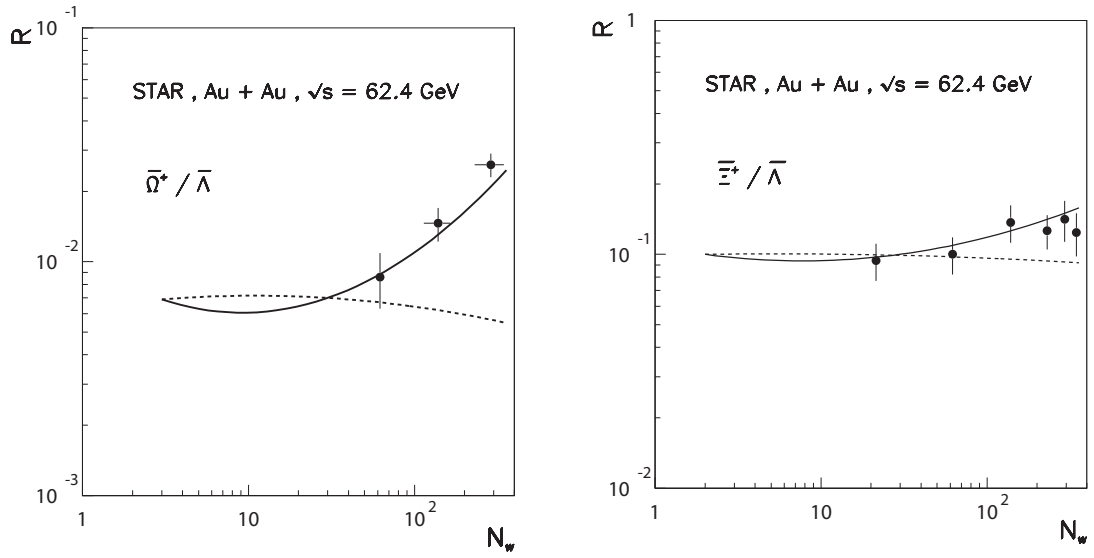


Figure 6: The experimental points obtained by the STAR Collaboration on the ratios of $\bar{\Omega}^+ / \bar{\Lambda}$ (left panel), and $\bar{\Xi}^+ / \bar{\Lambda}$ (right panel), in Au+Au collisions at $\sqrt{s} = 62.4$ GeV, at different centralities, as a function of the number of wounded nucleons, N_w , together with the results of the corresponding QGSM calculations (solid curves).

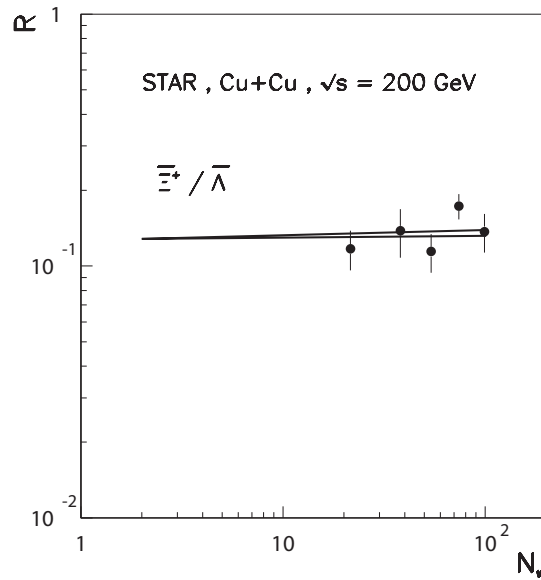


Figure 7: The experimental points obtained by the STAR Collaboration on the ratios $\bar{\Xi}^+ / \bar{\Lambda}$ in Cu+Cu collisions at $\sqrt{s} = 200$ GeV, at different centralities, as a function of the number of wounded nucleons, N_w , together with the results of the corresponding QGSM calculations.

4.3 LHC experimental data

In Table 4 we consider the experimental data on p , \bar{p} , and Ξ^- , $\bar{\Xi}^+$, Ω^- , $\bar{\Omega}^+$ production in central Pb+Pb collisions at $\sqrt{s}=2.76$ TeV, and of $p + \bar{p}$ production in central Pb+Pb collisions at $\sqrt{s}=5.02$ TeV, measured by the ALICE Collaboration [77, 78, 79], at the CERN LHC.

Process	\sqrt{s} (TeV)	Centrality	dn/dy (Experimental Data)	dn/dy (QGSM)	λ_s
Pb+Pb $\rightarrow p$	2.76	0–5%	34 ± 3 [77]	34.604	0,32
Pb+Pb $\rightarrow \bar{p}$	2.76	0–5%	33 ± 3 [77]	33.898	
Pb+Pb $\rightarrow p + \bar{p}$	5.02	0–5%	$74.56 \pm 0.06 \pm 3.75$ [79]	77.71	0,32
Pb+Pb $\rightarrow \Xi^-$	2.76	0–10%	$3.34 \pm 0.06 \pm 0.24$ [78]	3.357	0,32
Pb+Pb $\rightarrow \bar{\Xi}^+$	2.76	0–10%	$3.28 \pm 0.06 \pm 0.23$ [78]	3.317	
Pb+Pb $\rightarrow \Omega^-$	2.76	0–10%	$0,58 \pm 0.04 \pm 0.09$ [78]	0.606	0.38
Pb+Pb $\rightarrow \bar{\Omega}^+$	2.76	0–10%	$0,60 \pm 0.05 \pm 0.09$ [78]	0,601	

Table 4: Experimental data on dn/dy by the ALICE Collaboration of p , \bar{p} central production at $\sqrt{s}=2.76$ TeV [77], of $p+\bar{p}$ central production at $\sqrt{s}=5.02$ TeV [79], Ξ^- , and of Ξ^- , $\bar{\Xi}^+$, Ω^- , and $\bar{\Omega}^+$ production in central Pb+Pb collisions at $\sqrt{s}=2.76$ TeV per nucleon [78], and the comparison with the results of the corresponding QGSM calculations.

Here we can see that the strangeness suppression parameter λ_s for Ξ^- and $\bar{\Xi}^+$ production becomes smaller than at RHIC energies, taking the standard value $\lambda_s=0.32$. In the case of Ω^- and $\bar{\Omega}^+$ production, the value of λ_s also decreases with respect to the RHIC energy range. Thus we see that the unusually large values of λ_s for central Pb+Pb collisions at 158 GeV/c per nucleon, monotonically decrease with the increase of the initial energy of the collision.

5 Conclusion

We consider the production of hyperons in collisions on nuclear targets, in the frame of the QGSM formalism, and we find that one unexpected scenario appears when comparing the QGSM predictions with the available experimental data. Thus, while the experimental data on multistrange hyperon and antihyperon production in p -nucleus and in peripheral nucleus-nucleus collisions can be reasonably described by the QGSM, by using for all baryons the same standard value of the strange suppression parameter $\lambda_s=0.32$ (see Table 1 and figs. 3, 6, and 7), to get a correct description in QGSM of multistrange hyperon and antihyperon production in central Pb+Pb collisions in the midrapidity region, a larger value of λ_s is needed (as it can be seen in Table 2). In particular, in Fig. 3 one can see that the experimental probability of multistrange hyperon production in Pb+Pb collisions increases monotonically with the number of wounded nucleons, N_w , i.e. when in nucleus-nucleus going from peripheral to very central collisions.

A similar situation also occurs in the case of Au+Au collisions at RHIC energies (see Table 3 and Fig. 6), while in the case of Cu+Cu collisions this effect is practically negligible (see Table 3 and Fig. 7), probably because the Cu nucleus is not heavy enough.

Actually, the experimental data on the production of multistrange hyperons in central collisions of heavy nuclei show a very significant violation, essentially large at CERN-SPS energies $\sqrt{s}=17.3$ GeV, and that it decreases with the growth of the initial energy of the collision, of simple quark combinatorial rules [21, 22, 23], while, at the same time, the corresponding data in proton-nucleus and in peripheral nucleus-nucleus collisions are in agreement with the theoretical description based on those quark combinatorial rules.

We point out the remarkable experimental fact of the different strangeness suppression in multistrange hyperon production, from central collisions of heavy nuclei to proton-nucleus and peripheral nucleus-nucleus collisions, and the decreasing of this effect with the increase of the initial energy of the collision.

The full theoretical explanation, as well as the description of the corresponding microscopic mechanism, of this experimental effect are still to be formulated, what it will be crucial to determine if, and under which conditions, the reduction of strangeness suppression can be considered as an undisputed signature of the realization of the phase transition to QGP in high energy nuclear collisions.

Acknowledgements

This paper was supported by Ministerio de Economía, Industria y Competitividad, Spain (María de Maeztu Unit of Excellence MDM-2016-0692), and by Xunta de Galicia, Galiza-Spain (Consolidación e Estructuración 2021 GEC GI-2033-TEOFPACC).

References

- [1] A.B. Kaidalov and K.A. Ter-Martorisyan, Phys. Lett. **B117**, 247 (1982), doi:10.1016/0370-2693(82)90556-1.
- [2] A.B. Kaidalov and K.A. Ter-Martirosyan, Sov. J. Nucl. Phys. **39**, 979 (1984), Yad. Fiz. **39**, 1545 (1984); Sov. J. Nucl. Phys. **40**, 135 (1984), Yad. Fiz. **40**, 211 (1984).
- [3] A.B. Kaidalov, Sov. J. Nucl. Phys. **45**, 902 (1987), Yad. Fiz. **45**, 1452 (1987).
- [4] A.B. Kaidalov, Phys. Atom. Nucl. **66**, 1994 (2003), doi:10.1134/1.1625743, Yad. Fiz. **66**, 2044 (2003).
- [5] G.C. Rossi and G. Veneziano, Nucl. Phys. **B123**, 507 (1977), doi:10.1016/0550-3213(77)90178-X.
- [6] M. Ciafalloni, G. Marchesini and G. Veneziano, Nucl. Phys. **B98**, 472 (1975), doi:10.1016/0550-3213(75)90502-7.
- [7] V.N. Gribov, Sov. Phys. JETP **29**, 483 (1969), Zh. Eksp. Teor. Fiz. **56**, 892 (1969).
- [8] A. Capella, A. Kaidalov, and J. Tran Thanh Van, Acta Phys. Hung. **A9**, 169 (1999), e-Print:9903244[hep-ph].

- [9] A.B. Kaidalov and O.I. Piskounova, Sov. J. Nucl. Phys. **41**, 816 (1985), Yad. Fiz. **41**, 1278 (1985); Z. Phys. **C30**, 145 (1986), doi:10.1007/BF01560688.
- [10] Yu.M. Shabelski, Sov. J. Nucl. Phys. **44**, 117 (1986), Yad. Fiz. **44**, 186 (1986).
- [11] G.H. Arakelyan, A. Capella, A.B. Kaidalov, and Yu.M. Shabelski, Eur. Phys. J. **C26**, 81 (2002), doi:10.1007/s10052-002-0977-z, e-Print:0103337[hep-ph]
- [12] G.H. Arakelyan, C. Merino, C. Pajares, and Yu.M. Shabelski, Eur. Phys. J. **C54**, 577 (2008), doi:10.1140/epjc/s10052-008-0554-1, e-Print:0709.3174[hep-ph].
- [13] C. Merino, C. Pajares and Yu.M. Shabelski, Eur. Phys. J. **C71**, 1652 (2011), doi:10.1140/epjc/s10052-011-1652-z.
- [14] A.B. Kaidalov, K.A. Ter-Martirosyan, and Yu.M. Shabelski, Sov. J. Nucl. Phys. **43**, 822 (1986), Yad. Fiz. **43**, 1282 (1986).
- [15] Yu.M. Shabelski, Z. Phys. **C38**, 569 (1988), doi:10.1007/BF01624362.
- [16] G.H. Arakelyan, C. Merino, and Yu.M. Shabelski, Eur. Phys. J. **A52**, 9 (2016), doi:10.1140/epja/i2016-16009-2, e-Print:1509.05218[hep-ph].
- [17] Yu.M. Shabelski, Sov. J. Nucl. Phys. **50**, 149 (1989), Yad. Fiz. **50**, 239 (1989).
- [18] Yu.M. Shabelski, Z. Phys. **C57**, 409 (1993), doi:10.1007/BF01474336.
- [19] J. Dias de Deus and Yu.M. Shabelski, Phys. Atom. Nucl. **71**, 190 (2008), doi:10.1134/S1063778808010213, Yad. Fiz. **71**, 191 (2008), e-Print:0612346[hep-ph].
- [20] G.H. Arakelyan, C. Merino, and Yu.M. Shabelski, Phys. Atom. Nucl. **77**, 626 (2014), doi:10.1134/S1063778814050172, Yad. Fiz. **77**, 661 (2014), e-Print:1305.0388[hep-ph].
- [21] V.V. Anisovich and V.M. Shekhter, Nucl. Phys. **B55**, 455 (1973), doi:10.1016/0550-3213(73)90391-X, Nucl. Phys. **B63**, 542 (1973) (erratum), doi:10.1016/0550-3213(73)90163-6.
- [22] A. Capella and C.A. Salgado, Phys. Rev. **C60**, 054906 (1999), doi:10.1103/PhysRevC.60.054906, e-Print:9903414[hep-ph].
- [23] G.H. Arakelyan, A.B. Kaidalov, C. Merino, and Yu.M. Shabelski, Phys. Atom. Nucl. **74**, 126 (2011), doi:10.1134/S1063778811030057, and e-Print:1004.4074[hep-ph].
- [24] G. Bocquet *et al.*, UA1 Collaboration, Phys. Lett. **B366**, 447 (1996), doi:10.1016/0370-2693(95)01437-3.
- [25] Sa Ben-Tao and Tai An, Phys. Lett. **B399**, 29 (1997), doi:10.1016/S0370-2693(97)00274-8, e-Print:9804003[nucl-th].

- [26] H.-J. Drescher, J. Aichelin, and K. Werner, Phys. Rev. **D65**, 057501 (2002), doi:10.1103/PhysRevD.65.057501, e-Print:0105020[hep-ph].
- [27] A. Tounsi and K. Redlich, e-Print:0111159[hep-ph].
- [28] J.S. Hamieh, K. Redlich, and A. Tounsi, Phys. Lett. **B486**, 61 (2000), doi:10.1016/S0370-2693(00)00762-0, e-Print:0006024[hep-ph].
- [29] M. Bleicher, W. Greiner, H. Stöcker, and N. Xu, Phys. Rev. **C62**, 061901 (2000), doi:10.1103/PhysRevC.62.061901, e-Print:0007215[hep-ph].
- [30] E. Andersen *et al.*, WA97 Collaboration, Phys. Lett. **B449**, 401 (1999), doi:10.1016/S0370-2693(99)00140-9.
- [31] N. Carrer, NA57 and WA97 Collaborations, contribution to the Proceedings of the 16th International Conference on Strangeness in Quark Matter (Quark Matter 200i), Berkeley, CA (USA), 20-25 July 2000, J. Phys. **G27**, 391 (2001), doi:10.1088/0954-3899/27/3/317.
- [32] S. Kabana *e al.*, NA52 Collaboration, contribution to the Proceedings of the 16th International Conference on Strangeness in Quark Matter (Quark Matter 200i), Berkeley, CA (USA), 20-25 July 2000, J. Phys. **G27**, 495 (2001), doi:10.1088/0954-3899/27/3/329, e-Print:0010053[hep-ex].
- [33] F. Becattini *et al.*, Phys. Lett. **B632**, 233 (2006), doi:10.1016/j.physletb.2005.10.053, e-Print:0508188[hep-ph].
- [34] J. Cleymans, B. Kämpfer, and S. Wheaton, contribution to the Proceedings of the 16th International Conference on Ultra-Relativistic Nucleus-Nucleus Collisions (Quark Matter 2002), Nantes (France), 18-24 July 2002, Nucl. Phys. **A715**, 553 (2003), doi:10.1016/S0375-9474(02)01517-8, e-Print:0208247[hep-ph].
- [35] F. Becattini *et al.*, Phys. Rev. **C69**, 024905 (2004), doi:10.1103/PhysRevC.69.024905, e-Print:0310049[hep-ph].
- [36] O. Fochler *et al.*, contribution to the Proceedings of the 43rd International Winter Meeting in Nuclear Physics (Bormio 2005), Bormio (Italy), 13-20 March 2005, e-Print:050502[hep-ph].
- [37] S. Lobanov, A. Maevskiy, and L. Smirnova, contribution to the Proceedings of the International Workshop on the March (IHEP-LHC-2011), Protvino (Russian Federation), 16-18 November 2011, PoS IHEP-LHC-2011, **168**, 006 (2011), doi:10.22323/1.168.0008.
- [38] P.K. Malhotra and R. Orava, Z. Phys. **C17**, 85 (1983), doi:10.1007/BF01577823.

- [39] A. Wroblewski, *Acta Phys. Pol.* **B16**, 379 (1985).
- [40] H.-Y. Long *et al.*, *Phys. Rev* **C84**, 0349 (2011), doi:10.1103/PhysRevC.84.034905, e-Print:1103.2618[hep-ph].
- [41] K. Aamodt *et al.*, ALICE Collaboration, *Eur. Phys. J.* **C68**, 345 (2010), doi:10.1140/epjc/s10052-010-1350-2, e-Print:1004.3514[hep-ex], and references therein.
- [42] V. Khachatryan *et al.*, CMS Collaboration, *JHEP* **01**, 079 (2011), doi:10.1007/JHEP01(2011)079, e-Print:1011.5531[hep-ex], and references therein.
- [43] G. Aad *et al.*, ATLAS Collaboration, *New J. Phys.* **13**, 053033 (2011), doi:10.1088/1367-2630/13/5/053033, e-Print:1012.5104[hep-ex], and references therein.
- [44] H. Satz, *EPJ Web of Conferences* **171**, 02005 (2018), doi:10.1051/epjconf/201817102005.
- [45] V.A. Abramovsky, V.N. Gribov, and O.V. Kancheli, *Sov. J. Nucl. Phys.* **18**, 308 (1973), *Yad. Fiz.* **18**, 595 (1973).
- [46] A.B. Kaidalov, *Sov. J. Nucl. Phys.* **45**, 902 (1987), *Yad. Fiz.* **45**, 1452 (1987).
- [47] L. Bertocchi and D. Treleani, *J. Phys.* **G3**, 147 (1977), doi:10.1088/0305-4616/3/2/007.
- [48] J. Weis, *Acta Phys. Polon.* **B7**, 851 (1976).
- [49] Yu.M. Shabelski, *Sov. J. Nucl. Phys.* **26**, 573 (1977), *Yad. Fiz.* **26**, 1084 (1977), *Nucl. Phys.* **B132**, 491 (1978), doi:10.1016/0550-3213(78)90473-X.
- [50] T. Jaroszewicz, J. Kwiecinski, L. Lesniak, and K. Zalewski, *Z. Phys.* **C1**, 181 (1979), doi:10.1007/BF01445409.
- [51] G.D. Alkhalzov *et al.*, *Nucl. Phys.* **A280**, 365 (1977), doi:10.1016/0375-9474(77)90611-X.
- [52] B.B. Back *et al.*, PHOBOS Collaboration, *Phys. Rev. Lett.* **85**, 3100 (2000), doi:10.1103/PhysRevLett.85.3100, e-Print:0007036[hep-ex].
- [53] K. Adcox *et al.*, PHENIX Collaboration, *Phys. Rev. Lett.* **86**, 3500 (2001), doi:10.1103/PhysRevLett.86.3500, e-Print:0012008[nucl-ex].
- [54] A. Capella, C. Merino, and J. Tran Thanh Van, *Phys. Lett.* **B265**, 415 (1991), *Nucl. Phys* **A544**, 581 (1992), doi:10.1103/PhysRevD.45.92.

- [55] N. Armesto and C. Pajares, Int. J. Mod. Phys. **A15**, 2019 (2000), doi:10.1142/S0217751X00000823, e-Print:0002163[hep-ph].
- [56] A. Schwimmer, Nucl. Phys. **B94**, 445 (1975), doi:10.1016/0550-3213(75)90106-6.
- [57] N. S. Amelin, M. A. Braun, and C. Pajares, Phys. Lett. **B306**, 312 (1993), doi:10.1016/0370-2693(93)90085-V.
- [58] N. S. Amelin, M. A. Braun, and C. Pajares, Z. Phys. **C63**, 507 (1994), doi:10.1007/BF01580331.
- [59] N. Armesto, M.A. Braun, E.G. Ferreira, and C. Pajares, Phys. Rev. Lett. **77**, 3736 (1996), doi:10.1103/PhysRevLett.77.3736, e-Print:9607239[hep-ph].
- [60] G.H. Arakelyan, C. Merino, and Yu.M. Shabelski, Int. J. Mod. Phys. **A33**, 1850202 (2018), doi:10.1142/S0217751X18502020, e-Print:1810.02170[hep-ph].
- [61] G.H. Arakelyan, C. Merino, and Yu.M. Shabelski, Eur. Phys. J. **A55**, 151 (2019), doi:10.1140/epja/i2019-12832-1, e-Print:1805.11419[hep-ph].
- [62] T. Anticic *et al.*, NA49 Collaboration, Phys. Rev. **C69**, 024902 (2004), doi:10.1103/PhysRevC.69.024902.
- [63] T. Anticic *et al.*, NA49 Collaboration, Phys. Rev. Lett. **93**, 022302 (2004), doi:10.1103/PhysRevLett.93.022302, e-Print:0311024[nucl-ex].
- [64] C. Alt *et al.*, NA49 Collaboration, Phys. Rev. Lett. **94**, 192301 (2005), doi:10.1103/PhysRevLett.94.192301, e-Print:0409004[nucl-ex].
- [65] C. Alt *et al.*, NA49 Collaboration, Phys. Rev. **C78**, 034918 (2008), doi:10.1103/PhysRevC.78.034918, e-Print:0804.3770[nucl-ex].
- [66] T. Anticic *et al.*, NA49 Collaboration, Phys. Rev. **C80**, 034906 (2009), doi:10.1103/PhysRevC.80.034906, e-Print:0906.0469[nucl-ex].
- [67] C. Blume and C. Markert, Prog. Part. Nucl. Phys. **66**, 834 (2011), doi:10.1016/j.pnpnp.2011.05.001, e-Print:1105.2798[nucl-ex].
- [68] F. Antinori *et al.*, NA57 Collaboration, Phys. Lett. **B595**, 68 (2004), doi:10.1016/j.physletb.2004.05.025, e-Print:0403022[nucl-ex].
- [69] F. Antinori *et al.*, NA57 Collaboration, J. Phys. **G32**, 427 (2006), doi:10.1088/0954-3899/32/4/003, e-Print:0601021[nucl-ex].
- [70] J. Adams *et al.*, STAR Collaboration, Phys. Rev. Lett. **92**, 182301 (2004), doi:10.1103/PhysRevLett.92.182301, e-Print:0307024[nucl-ex].

- [71] J. Adams *et al.*, STAR Collaboration, Phys. Rev. Lett. **98**, 062301 (2007), doi:10.1103/PhysRevLett.98.062301, e-Print:0606014[nucl-ex].
- [72] B.I. Abelev *et al.*, STAR Collaboration, Phys. Rev. **C79**, 034909 (2009), doi:10.1103/PhysRevC.79.034909, e-Print:0808.2041[nucl-ex].
- [73] M.M. Aggarwal *et al.*, STAR Collaboration, Phys. Rev. **C83**, 024901 (2011), doi:10.1103/PhysRevC.83.024901, e-Print:1010.0142[nucl-ex].
- [74] G. Agakishiev *et al.*, STAR Collaboration, Phys. Rev. Lett. **108**, 072301 (2012), doi:10.1103/PhysRevLett.108.072301, e-Print:1107.2955[nucl-ex].
- [75] K. Adcox *et al.*, PHENIX Collaboration, Phys. Rev. Lett. **89**, 092302 (2002), doi:10.1103/PhysRevLett.89.092302, e-Print:0204007[nucl-ex].
- [76] K. Adcox *et al.*, PHENIX Collaboration, Phys. Rev. **C69**, 024904 (2004), doi:10.1103/PhysRevC.69.024904, e-Print:0307010[nucl-ex].
- [77] B. Abelev *et al.*, ALICE Collaboration, Phys. Rev. **C88**, 044910 (2013), doi:10.1103/PhysRevC.88.044910, e-Print:1303.0737[hep-ex].
- [78] B. Abelev *et al.*, ALICE Collaboration, Phys. Lett. **B728**, 216 (2014), doi:10.1016/j.physletb.2013.11.048, Phys. Lett. **B734**, 409 (2014) (erratum), doi:10.1016/j.physletb.2014.05.052, e-Print:1307.5543[nucl-ex].
- [79] S. Acharya *et al.*, ALICE Collaboration, Phys. Rev. **C101**, 044907 (2020), doi:10.1103/PhysRevC.101.044907, e-Print:1910.07678[nucl-ex].